Magnetic structure in iron borates $RFe_3(BO_3)_4$ (R = Er, Pr): a neutron diffraction and magnetization study

2010 J. Phys.: Condens. Matter 22 206002

(http://iopscience.iop.org/0953-8984/22/20/206002)

J. Phys.: Condens. Matter **22** (2010) 206002 (8pp) doi:10.1088/0953-8984/22/20/206002

Magnetic structure in iron borates $RFe_3(BO_3)_4$ (R = Er, Pr): a neutron diffraction and magnetization study

C Ritter[1], A Vorotynov[2], A Pankrats[2], G Petrakovskiĭ[2,3], V Temerov[2], I Gudim[2] and R Szymczak[4]

[1] Institut Laue-Langevin, Boite Postale 156, F-38042 Grenoble, France
[2] L V Kirenskii Institute of Physics, Siberian Branch of RAS, Krasnoyarsk 660036, Russia
[3] Siberian Federal University, Krasnoyarsk, Russia
[4] Institute of Physics PAS, Warsaw, Poland

E-mail: ritter@ill.fr

Received 4 March 2010, in final form 1 April 2010
Published 26 April 2010
Online at stacks.iop.org/JPhysCM/22/206002

Abstract

Neutron diffraction, susceptibility and magnetization measurements (for R = Er only) were performed on iron borates $RFe_3(BO_3)_4$ (R = Pr, Er) to investigate details of the crystallographic structure, the low temperature magnetic structures and transitions and to study the role of the rare earth anisotropy. $PrFe_3(BO_3)_4$, which crystallizes in the spacegroup $R32$, becomes antiferromagnetic at $T_N = 32$ K, with $\tau = [0\ 0\ 3/2]$, while $ErFe_3(BO_3)_4$, which keeps the $P3_121$ symmetry over the whole studied temperature range 1.5 K $< T <$ 520 K, becomes antiferromagnetic below $T_N = 40$ K, with $\tau = [0\ 0\ 1/2]$. Both magnetic propagation vectors lead to a doubling of the crystallographic unit cell in the c-direction. Due to the strong polarization of the Fe-sublattice, the magnetic ordering of the rare earth sublattices appears simultaneously at T_N. The moment directions are determined by the rare earth anisotropy: easy-axis along c for $PrFe_3(BO_3)_4$ and easy-plane a–b for $ErFe_3(BO_3)_4$. There are no spin reorientations present in either of the two compounds but there is the appearance below 10 K of a minority phase in the Er-compound adopting a 120° arrangement of the Er-moments.

(Some figures in this article are in colour only in the electronic version)

1. Introduction

Due to their interesting magnetic, magnetoelectric and multiferroic properties considerable research effort has been put in recent years into the study of the family of rare earth ferroborates with the general formula $RFe_3(BO_3)_4$ [1–5]. The presence of two magnetic sublattices and a crystal structure which is strongly determined by one-dimensional structure elements make these compounds interesting not only for practical applications but also from a purely theoretical point of view when studying the different possible magnetic interactions. Information on the magnetic ground state or the magnetic field induced magnetic structure in these compounds was first deduced from macroscopic magnetic or spectroscopic methods [6–10] before the microscopic methods of neutron diffraction and magnetic x-ray scattering gave direct insight into the details of the magnetic order [11–14].

Depending on the rare earth ionic radius, these compounds crystallize either in spacegroup $R32$ or $P3_121$ possessing a single rare earth site and one ($R32$) or two ($P3_121$) independent iron sites [15, 16]. Common to both structures is the presence of 1D helicoidal chains of FeO_6 octahedra parallel to the c-axis with intrachain Fe–Fe distances significantly shorter than interchain Fe–Fe distances. Large trigonal prisms of RO_6 are placed in a way so as to connect three different chains. There are no R–O–R links and the R ions are only coupled by indirect R–O–Fe interactions. A detailed description and a picture of the structure can be found in Campá *et al* [17].

The competition of the temperature dependent contributions of the Fe- and R-sublattices to the total magnetic anisotropy of the crystal determines not only an easy-plane or easy-axis orientation of the spins but leads as well to spin reorientations and metamagnetic transitions. Our own neutron

data on compounds where R = Tb, Ho and Y [12, 13] as well as the first neutron diffraction data on $NdFe_3(BO_3)_4$ [11] found the simultaneous appearance of magnetic order on the rare earth and iron sublattices with magnetic structures characterized by an antiferromagnetic order leading to a doubling of the crystallographic unit cell in the *c*-direction. The neutron diffraction data as well as the magnetic data point to an easy-plane orientation of the magnetic sublattices in the Y- and the Nd-compounds while the easy-axis orientation is found for R = Tb over the whole temperature range below T_N and for R = Gd [18, 6] and Ho [13] below the spin reorientation temperature.

In these $RFe_3(BO_3)_4$ compounds the temperature of the structural transition from $R32$ to $P3_121$ as well as the temperature of the transition to the magnetically ordered state are directly related to the ionic radius of the R^{3+} ion [15]. As neutron diffraction using thermal neutrons is not possible on compounds containing the strongly absorbing elements Gd, Sm or Eu we decided to perform a study on the compounds $PrFe_3(BO_3)_4$ and $ErFe_3(BO_3)_4$ which represent, in the series known so far, the compounds with the largest (Pr^{3+}) and the smallest (Er^{3+}) ionic radius. Magnetic data on these two compounds indicate an easy-axis orientation for $PrFe_3(BO_3)_4$ [3] and an easy-plane orientation for $ErFe_3(BO_3)_4$ [8] with the direct determination of the magnetic structures using microscopic methods still missing. The unique contribution neutron diffraction can provide to the study of the magnetism of the $RFe_3(BO_3)_4$ series becomes clear when it is realized that, for example, only a detailed knowledge of the magnetic structure of $HoFe_3(BO_3)_4$ allowed us to couple the direction of the intrinsic polarization in this compound to the moment orientation of one of the two Fe-sublattices [5].

2. Experimental details

2.1. Sample preparation

Samples were prepared at the Institute of Physics at Krasnoyarsk. Because of the strong neutron absorption by natural boron, crystals of (Er, Pr)$Fe_3(BO_3)_4$ with ^{11}B enriched to 99% were grown. $ErFe_3(^{11}BO_3)_4$ and $PrFe_3(^{11}BO_3)_4$ single crystals were grown, respectively, from fluxes of 76.7 mass%($Bi_2Mo_3O_{12}$ + 3.14$^{11}B_2O_3$ + 0.54Er_2O_3) + 23.3 mass%$ErFe_3(^{11}BO_3)_4$ and 76.5 mass%($Bi_2MO_3O_{12}$ + 3$^{11}B_2O_3$ + 0.6Pr_2O_3) + 23.5 mass%$PrFe_3(^{11}BO_3)_4$. The fluxes with mass of 100 g were prepared by melting at a temperature of 1100 °C the oxides Bi_2O_3, MoO_3, $^{11}B_2O_3$, Fe_2O_3 and Er_2O_3 or Pr_2O_3 in a platinum crucible. In these fluxes the trigonal $ErFe_3(^{11}BO_3)_4$ and $PrFe_3(^{11}BO_3)_4$ are the high temperature phases and crystallize in the $T \approx 945$–900 °C interval. Crystals with linear dimensions of 5–7 mm were grown in the temperature decreasing regime. The growth speed did not exceed 1 mm day^{-1}. Samples for the magnetic and powders for the neutron measurements were prepared from grown crystals.

2.2. Magnetization and neutron diffraction measurements

Neutron diffraction data were taken at the Institut Laue-Langevin in Grenoble, France, using the high resolution powder diffractometer D1A (λ = 1.91 Å) and the high flux powder diffractometer D1B (λ = 2.52 Å). The temperature dependence of the neutron spectra of $ErFe_3(BO_3)_4$ was measured on D1B between 1.5 and 60 K with a temperature resolution of about 1 K taking a spectrum every 10 min in order to track any possible transition. High resolution data were then taken on D1A every 1 K between 1.5 and 15 K, then every 2 K up to 43 K as well as at 50 and 300 K. One additional data point was collected using λ = 1.39 Å at 520 K in order to check for a possible structural transition to $R32$. The Pr-compound was exclusively studied on D1A: between 1.5 and 35 K spectra were taken every degree with additional data points at 50, 100, 200 and 300 K. The spectra were refined by the Rietveld method using the FULLPROF [19] program.

The magnetic properties of a $ErFe_3(BO_3)_4$ single crystal were studied at temperatures of 2–300 K in magnetic fields up to 5 T by a superconducting quantum interference device (SQUID) magnetometer MPMS-5 at the Institute of Physics PAS (Warsaw).

3. Results and discussion

Data taken at 300 K were used to verify the room temperature crystal structure and the purity of the two compounds. No impurity phases are present in either of the samples and as expected $ErFe_3(BO_3)_4$ adopts the $P3_121$ spacegroup while $PrFe_3(BO_3)_4$ crystallizes in $R32$. Table 1 displays the results of the room temperature refinement of the two compounds and gives the most important interatomic distances and angles. It has to be noted that the increase of the unit cell parameters when going from the Er- to the Pr-compound is of the order of $\delta a/a = 0.8\%$, $\delta c/c = 1\%$ leading to a volume increase of nearly 3%. This volume increase is, however, not isotropic within the unit cell. While the size of the RO_6 prisms increases by about 9%, the Fe–Fe distance along the helicoidal chain increases only by about 0.3%. This confirms the role of this helicoidal chain as the 'backbone' of the structure and might explain the relatively small differences between the magnetic transition temperatures in the $RFe_3(BO_3)_4$ compounds [15].

The refinement of the data taken at 520 K on $ErFe_3(BO_3)_4$ indicates that even at this high temperature, and 20 K above the estimated transition temperature following [15], the compound is still crystallizing in $P3_121$. This is in contradiction to the data of Fausti *et al* [20] who found a transition temperature of only about 340 K. The authors of [20] had already pointed out the necessity to verify this result of their single crystal study after having stated the apparent contradiction to [15].

Figure 1 shows for $2\Theta < 60°$ the thermal dependence of the neutron diffraction pattern (thermodiffractogram) of $PrFe_3(BO_3)_4$ between 1.5 and 40 K. The appearance of new reflections on cooling down can be clearly seen at about 32 K. These reflections are of magnetic origin and can be indexed with the propagation vector $\tau = [0, 0, 3/2]$ as already found in $NdFe_3(BO_3)_4$ [11]. Here we assumed that the Pr-compound

Table 1. Structural data at 1.5 and 300 K of $PrFe_3(BO_3)_4$ refined in $R32$ and $ErFe_3(BO_3)_4$ refined in $P3_121$ together with the most important interatomic distances.

$P3_121$	Pr 1.5 K	300 K	1.5 K	Er 300 K		$R32$
a (Å)	9.506 82(6)	9.514 76(10)	9.514 32(5)	9.530 67(5)		a (Å)
c (Å)	7.533 26(8)	7.544 44(12)	7.539 33(9)	7.555 27(6)		c (Å)
RE (3a) x	0.3372(11)	0.3350(11)				
Fe1 (3a) x	0.8836(9)	0.8820(8)	0.5507(2)	0.5510(2)	x	Fe (9d)
Fe2 (6c) x	0.7887(6)	0.7846(6)				
y	0.4512(6)	0.4507(6)				
z	0.3452(6)	0.3435(6)				
O1 (3b) x	0.9238(13)	0.9187(10)	0.8542(4)	0.8546(4)	x	O1 (9e)
O2 (6c) x	0.4202(10)	0.4122(9)	0.5904(3)	0.5896(3)	x	O2 (9e)
y	0.7229(9)	0.7173(8)				
z	0.1237(8)	0.1289(7)				
O3 (6c) x	0.8746(11)	0.8720(10)	0.0262(2)	0.0266(2)	x	O3 (18f)
y	0.6913(14)	0.6945(12)	0.2149(2)	0.2152(2)	y	
z	0.8250(14)	0.8236(13)	0.1863(2)	0.1861(2)	z	
O4 (6c) x	0.8537(12)	0.8606(10)				
y	0.6383(12)	0.6391(10)				
z	0.1872(14)	0.1893(13)				
O5 (6c) x	0.4735(9)	0.4767(8)				
y	0.1422(12)	0.1495(12)				
z	0.8443(14)	0.8419(15)				
O6 (3b) x	0.1839(14)	0.1874(14)				
O7 (6c) x	0.4753(9)	0.4818(9)				
y	0.4651(11)	0.4675(10)				
z	0.8146(11)	0.8138(12)				
B1 (3b) x	0.3306(15)	0.3347(15)				
B2 (6c) x	0.5505(11)	0.5565(11)	0.4459(2)	0.4455(2)	x	B2 (9e)
y	0.8757(15)	0.8814(9)				
z	0.1472(9)	0.1562(13)				
B3 (3b) x	0.7807(15)	0.7871(15)				
Fe1–Fe1 (Å)	3.159(6)	3.175(7)	3.185(1)	3.186(1)		Fe–Fe (Å)
Fe2–Fe2 (Å)	3.195(7)	3.179(6)				
2 × Tb–O3 (Å)	2.31(1)	2.28(1)	2.409(2)	2.410(2)		6 × Tb–O3 (Å)
2 × Tb–O4 (Å)	2.40(2)	2.45(1)				
2 × Tb–O7 (Å)	2.31(1)	2.30(1)				

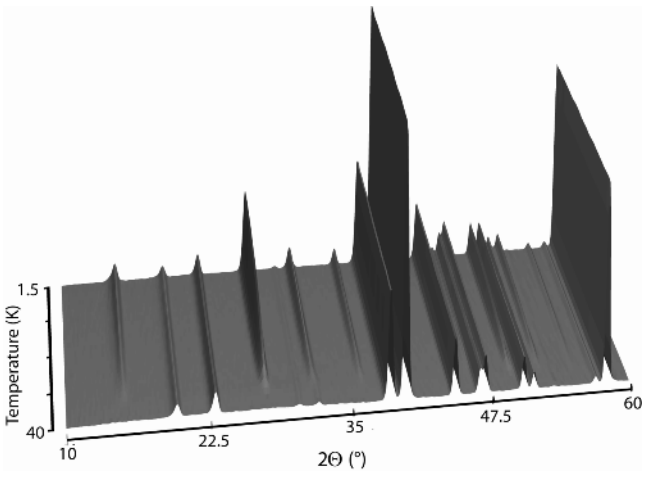

Figure 1. Thermal dependence of the neutron diffraction pattern (thermodiffractogram) of $PrFe_3(BO_3)_4$ between 1.5 and 40 K showing the appearance of new magnetic Bragg peaks at about 32 K; $\lambda = 1.91$ Å.

conserves as $NdFe_3(BO_3)_4$ the $R32$ symmetry down to lowest temperatures. In the light of the work of Hinatsu *et al* [15] this is reasonable as the ionic radius of Pr^{3+} is even larger than that of Nd^{3+}. This leads to a doubling of the magnetic unit cell in the c-direction compared to the nuclear unit cell. The thermodiffractogram does not give any indication of a spin reorientation as the growth of the magnetic peaks is uniform and steady.

Magnetic symmetry analysis as implemented in the program BASIREPS which is part of the FULLPROF suite of programs [19] was used to determine the two possible magnetic sites (Fe and Pr) and the allowed irreducible representations (IR) for this propagation vector in $R32$. The three allowed IRs were tested by refinement against the measured data. It was found that only the basis vectors of one IR are describing the magnetic arrangement correctly. Table 2 lists the basis vectors of this IR and the refined values of the three coefficients of the basis vectors for the data at 1.5 K; figure 2 shows a plot of the refined data in $R32$ and table 1 the crystallographic data.

The magnetic structure found resembles strongly those already found for $TbFe_3(BO_3)_4$ and for $HoFe_3(BO_3)_4$ below 6 K. The Fe-spins ($\mu_{Fe} = 4.30(3)\ \mu_B$) are coupled antiferromagnetically along the helicoidal chain running in the c-direction. The spin moments are pointing nearly exclusively along the c-direction adopting the easy-axis orientation. Within the hexagonal layers neighbouring Fe-spins are aligned

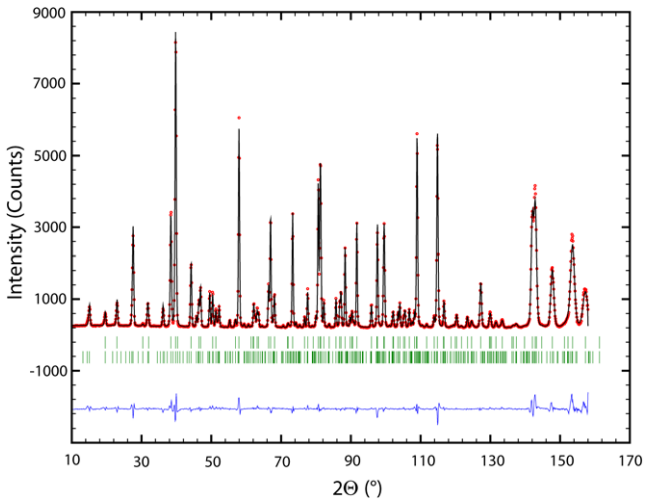

Figure 2. Observed (dots, red), calculated (line, black) and difference pattern of $PrFe_3(BO_3)_4$ at 1.5 K refined in $R32$. The tick marks indicate the calculated position of the nuclear (upper row) and magnetic (lower row) Bragg peaks.

Table 2. Basis vectors (BV) of the irreducible representation 2 for $\tau = [0, 0, 3/2]$ in $R32$. Refined values of their coefficients determined from the refinement of the magnetic structure of $PrFe_3(BO_3)_4$ at 1.5 K.

	BV1	BV2
Fe on x 0 0		
x, y, z	0.5 1 0	0 0 1
$-y, x-y, z$	-1 -0.5 0	0 0 1
$-x+y, -x, z$	0.5 0.5 0	0 0 1
Coefficient	0.2(1)	4.32(3)
Pr on 0 0 0		
x, y, z	0 0 1	
Coefficient	0.79(6)	

in parallel. The ordered magnetic moment value found for the Pr-site is with $\mu_{Pr} = 0.79(1)\ \mu_B$ quite small. Figure 3 displays this magnetic structure where the size of the Pr-moment has been exaggerated. Contrary to the case of the Tb- and the Ho-compounds, the magnetic moment of the rare earth sublattice in $PrFe_3(BO_3)_4$ is oriented parallel to the Fe-sublattice within the hexagonal layers. It is tempting to attribute this change of relative orientation between the rare earth and the iron sublattice within one layer to the fact that while Tb and Ho are heavy lanthanides, Pr is a light lanthanide. Postulating an antiferromagnetic indirect exchange interaction between the 3d band of iron and the 5d band of the rare earths this would lead through the 5d–4f exchange to a parallel alignment of the 4f electrons relative to the iron spins for rare earths having $J = |L - S|$ and an antiparallel alignment for rare earths with $J = |L + S|$. One has to realize, however, that the indirect Fe–O–R exchange interactions are coupling only iron and rare earth moments of neighbouring a–b-planes (figure 10 of [12]) which are in fact aligned antiparallel and that, therefore, the above picture must be wrong. There are no exchange interactions of type Fe–O–R within one layer. Very interesting in this context are the calculations of Popova *et al* [21] performed for $NdFe_3(BO_3)_4$ which show that the

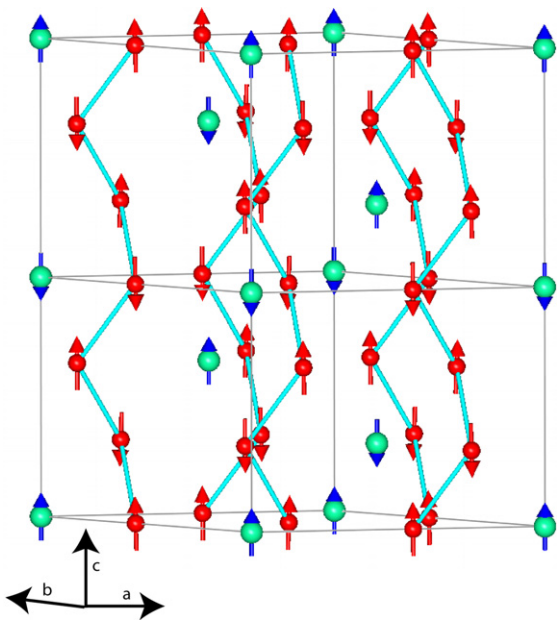

Figure 3. Magnetic structure of $PrFe_3(BO_3)_4$. Pr-moments in blue, Fe-spins in red, the direct Fe–Fe exchange along the helicoidal chains is indicated by light grey (blue) lines.

exchange between the magnetic moments on Fe^{3+} and Nd^{3+} is ferromagnetic as far as the spin part of the total moment $J = S + L$ is concerned. This leads through the spin–orbit coupling to an antiferromagnetic coupling between the iron spins and the neodymium moments. Assuming the same coupling mechanism to be valid as well in the other $RFe_3(BO_3)_4$ compounds the determined relative orientations between Fe-sublattice and R-sublattice are explained. Discussing the exchange interactions between the iron and the rare earth sublattice, one has to realize that the small value found for the magnetic moment of Pr points to a nearly singlet ground state of the non-Kramers ion Pr^{3+} in the crystal field.

The temperature dependence of the magnetic moments was determined by cyclic refinement of the neutron data using the same model which was used for the data at 1.5 K. The fact that the fits proceed smoothly up to the transition temperature $T_N = 32$ K excludes the existence of a spin reorientation as already conjectured from the visual inspection of the thermodiffractogram (figure 1). It is not possible to fit the thermal dependence of the Fe-moment with a Brillouin function with $J = 5/2$ correctly. This points to the fact that the magnetic behaviour of the Fe-sublattice in $PrFe_3(BO_3)_4$ is strongly determined by its interaction with the rare earth sublattice even if the total moment on the Pr-site amounts only to about 0.8 μ_B. The onset of the small magnetic moment at the Pr-site is simultaneous to the onset of the Fe-moment.

The occurrence of a magnetic moment on the rare earth sites depends—due to the absence of direct exchange interactions between the rare earths—on the polarizing effect of the magnetic Fe-sublattice. From $YFe_3(BO_3)_4$ we know that the anisotropy of the Fe-sublattice leads to an easy-plane state in the absence of a magnetic rare earth. The easy-axis orientation of the magnetic moments found in $PrFe_3(BO_3)_4$

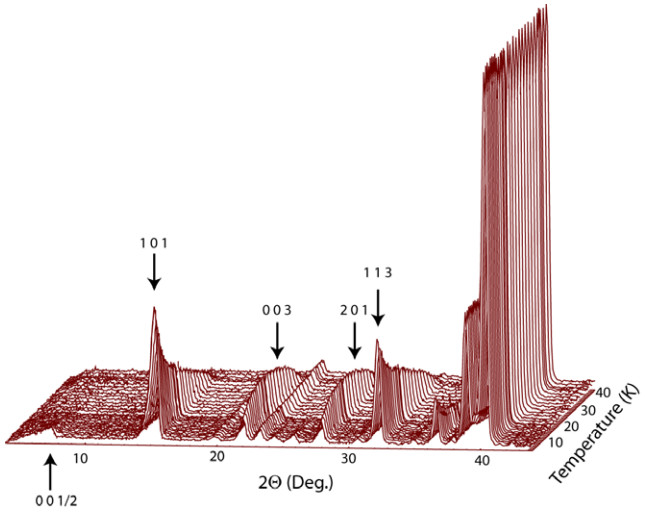

Figure 4. Thermal dependence of the neutron diffraction pattern (thermodiffractogram) of $ErFe_3(BO_3)_4$ between 1.5 and 43 K showing the appearance of new magnetic Bragg peaks at about 40 K, a decrease of the (0, 0, 3) and (2, 0, 1) peaks at about 15 K and the appearance of the (0, 0, 1/2) peaks at about 10 K; $\lambda = 1.91$ Å.

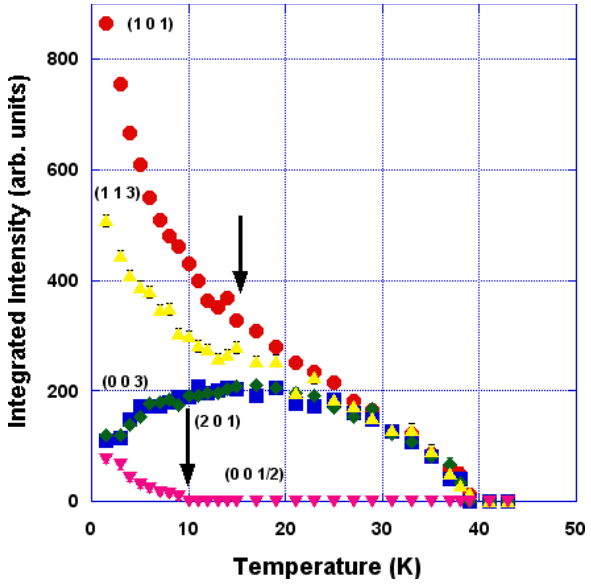

Figure 5. Integrated intensity of several characteristic magnetic Bragg peaks as a function of temperature. Arrows mark the occurrence of the (0, 0, 1/2) peak at 10 K and the temperature where changes in the slope appear at about 15 K.

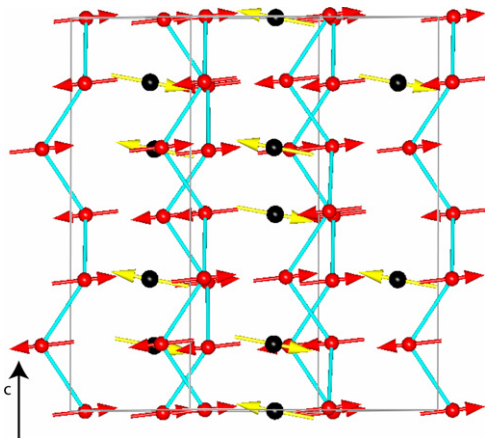

Figure 6. Main magnetic structure of $ErFe_3(BO_3)_4$. Er-moments in yellow, Fe-spins in red. Shown is the view along the *c*-direction of one magnetic unit cell.

together with the absence of a spin reorientation up to T_N and the presence of a small moment at the Pr-site appearing simultaneously with the Fe-moment at T_N let us conclude therefore that the influence of the anisotropy of the Pr-subsystem is already predominant at T_N. This has to be compared to the situation in other $RFe_3(BO_3)_4$ compounds which adopt an easy-axis orientation at low temperatures. In $GdFe_3(BO_3)_4$ as well as in $HoFe_3(BO_3)_4$ the anisotropy of the Fe-sublattice is dominant at T_N and only the increase of the temperature dependent contribution of the rare earth anisotropy leads at lower temperatures via a spin reorientation to an easy-axis orientation. The situation found in $PrFe_3(BO_3)_4$ is only realized in $TbFe_3(BO_3)_4$ as well where an easy-axis orientation is adopted right at T_N.

Figure 4 displays the thermodiffractogram as recorded for $ErFe_3(BO_3)_4$ between 1.5 and 43 K. The plot is again limited to the low 2Θ region so as to highlight the changes introduced by the magnetic scattering. Visible is the occurrence of new reflections at about 40 K. Some of these new reflections, e.g. the (0, 0, 3) and (2, 1, 0) peaks, decrease again at about 15 K. At low angles we note, furthermore, the appearance of a magnetic peak indexed as (0, 0, 1/2) using the spacegroup $P3_121$ which is valid for $ErFe_3(BO_3)_4$. A plot of the integrated intensities of various magnetic peaks is shown in figure 5. It shows that while the decrease of the (0, 0, 3) and (2, 1, 0) peaks starts at about 15 K the appearance of the new magnetic peak (0, 0, 1/2) happens only below 10 K. This indicates that we are in the presence of two different magnetic ordering phenomena.

All magnetic reflections, above and below 10 K, can be indexed with a magnetic propagation vector $k = [0, 0, 1/2]$ leading to a doubling of the magnetic unit cell in the *c*-direction compared to the crystallographic one. Refinement of the data above 10 K proceeds smoothly using the collinear model as already found for $HoFe_3(BO_3)_4$ above 6 K [13] where the Fe-sublattice is ordered in an easy-plane orientation and the rare earth sublattice couples antiparallel within one layer of the hexagonal *a*–*b*-plane. Only the Fe-sublattice sees a small out of plane contribution $\mu_{Fe\|c} < 1.0\ \mu_B$. At 10 K the total moment of iron amounts to about $\mu_{Fe} = 4.1\ \mu_B$ and that of erbium to about $\mu_{Er} = 2.2\ \mu_B$; figure 6 displays the magnetic structure found above 10 K.

Below 10 K the changes of the magnetic structure which lead to the appearance of the (0 0 1/2) peak as seen in figures 4 and 5 are solely determined by changes in the magnetic arrangement within the Er-sublattice. A new coupling leads to an arrangement where the Er-moments have an angle of 60° to each other when going from one *a*–*b*-plane to the neighbouring one. This represents the same arrangement as already found in $HoFe_3(BO_3)_4$ below 6 K [13]. It is described by a basis vector of an irreducible representation which also contains

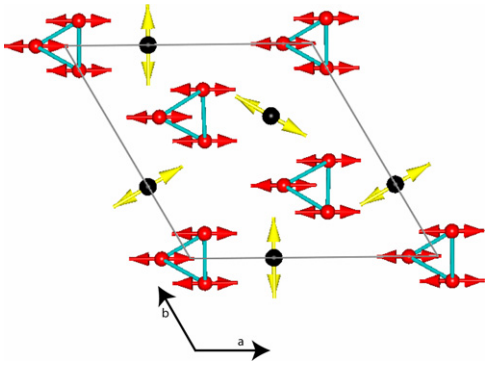

Figure 7. '120° structure' of the Er-sublattice (see text) as adopted in about 10% of the sample volume at 1.5 K.

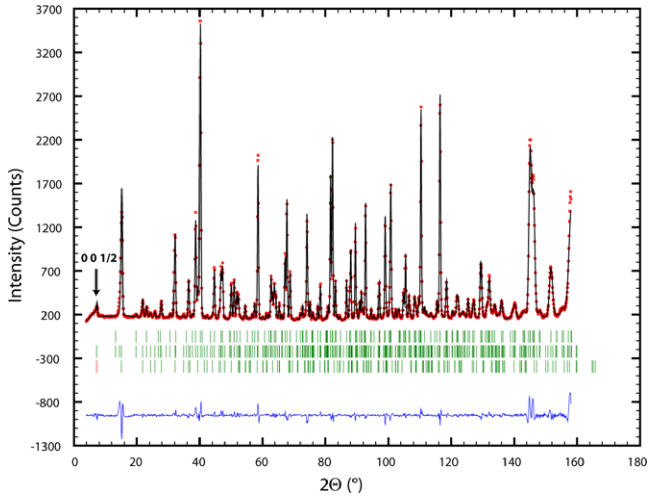

Figure 8. Observed (dots, red), calculated (line, black) and difference pattern of $ErFe_3(BO_3)_4$ at 1.5 K refined in $R32$.

a basis vector allowing an alignment of both sublattices in the c-direction. Opposite to the case of $HoFe_3(BO_3)_4$ below 6 K we see, however, in $ErFe_3(BO_3)_4$ no indication of a spin reorientation into this c-direction. The collinear magnetic structure as found above 10 K remains the main magnetic arrangement. Figure 7 displays this additional disposition of the Er-moments which we term the '120° structure' as it leads to a 120° arrangement of the antiferromagnetically coupled spins in the c-direction. Figure 8 shows the plot of the refined data at 1.5 K; table 1 shows the crystallographic details of the fit.

Refining the neutron diffraction data sequentially it is possible to follow the temperature dependence of the magnetic moment of the Fe-sublattice and of the Er-moments involved in the collinear and in the 120° structure magnetic arrangements (figure 9). Several facts become immediately clear when regarding figure 9: the onset of the magnetic order at $T_N = 40$ K is simultaneous for both sublattices. The thermal dependence of the Fe-sublattice magnetic moment does not follow a Brillouin function with $J = 5/2$. As in the case of the Pr-compound this is due to the interaction with the Er-sublattice. The Er-sublattice magnetization itself shows an almost linear increase between 40 and 15 K as it is not

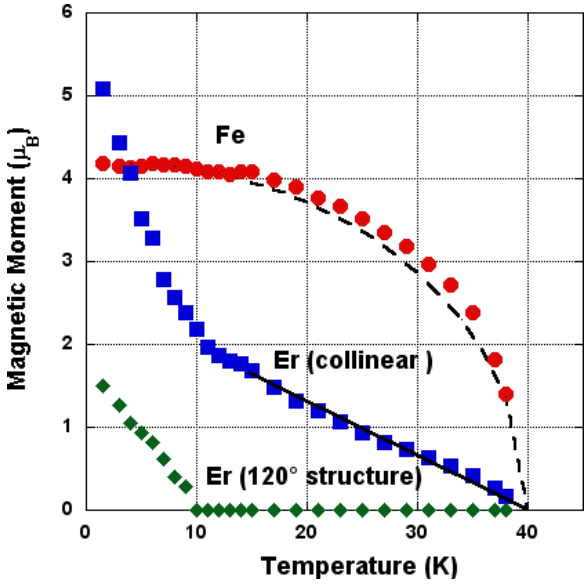

Figure 9. Temperature dependence of the magnetic moment values of the Fe-sublattice (circles) and of the Er-sublattice participating in the collinear main magnetic structure (squares) or in the 120° structure (diamonds). For the fit it was supposed that the collinear and the 120° structures are part of the same magnetic phase. The full curve is a fit to the temperature dependence of the Fe magnetic moment with the Brillouin function using $J = 5/2$.

governed by a simple exchange interaction between Er ions but is directly polarized by the Fe-sublattice. The magnetic moment value of the Fe-sublattice has practically reached its maximum value ($\mu_{Fe} = 4.2\ \mu_B$ at 1.5 K) at about 15 K and stays nearly constant below this temperature. At the same time the magnetic moment value of the Er-sublattice continues to increase. As the intensity of the magnetic peaks is determined by the magnetic structure factors of both sublattices, which can add or subtract the different temperature dependences of the two magnetic sublattices, it causes the decrease of the (0, 0, 3) and (2, 1, 0) peaks seen at 15 K (while (1 0 1) and (1 0 3) continue to increase). Figure 9 shows, furthermore, that the onset of the 120° structure at about 10 K also goes in parallel with a strong increase of the Er-moment participating in the collinear arrangement. At the lowest measured temperature of 1.5 K the increase of the ordered Er-moment is far from having reached its maximum value. As there is no appearance of a magnetic component in the c-direction, the transition starting at 10 K should not ultimately lead to a spin reorientation into an easy-axis type structure.

The presence of two different magnetic arrangements within the hexagonal a–b-plane acting on the Er-sublattice is intriguing. If coexisting over the whole sample volume (as assumed for the sequential refinement shown in figure 9) this would lead to some kind of amplitude modulated structure not found before in any of the $RFe_3(BO_3)_4$ compounds. More probable is the coexistence of two magnetic phases in spatially separated parts of the sample volume. The relative phase percentages can then be calculated assuming that the Er-moment value is equal in both phases and would amount to 98.5%/1.5%, 94%/6% and 92%/8% at 9 K, 5 K and

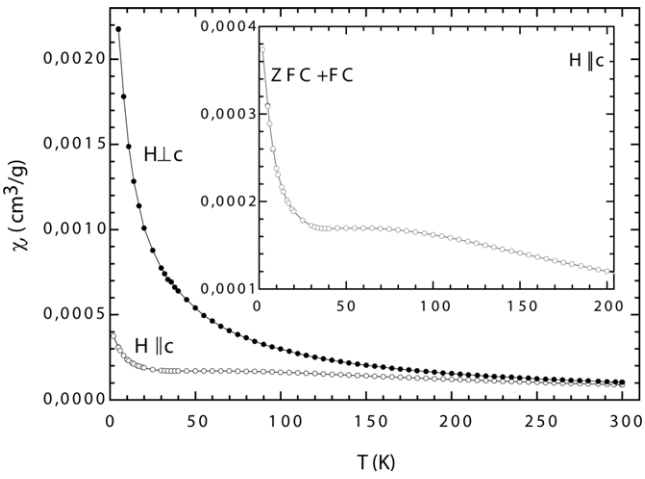

Figure 10. Temperature dependences of the magnetic susceptibilities of $ErFe_3(BO_3)_4$ measured at $H \parallel c$ and $H \perp c$. Inset: enlargement of the dependence for $H \parallel c$ measured with field-cooling and zero-field-cooling conditions.

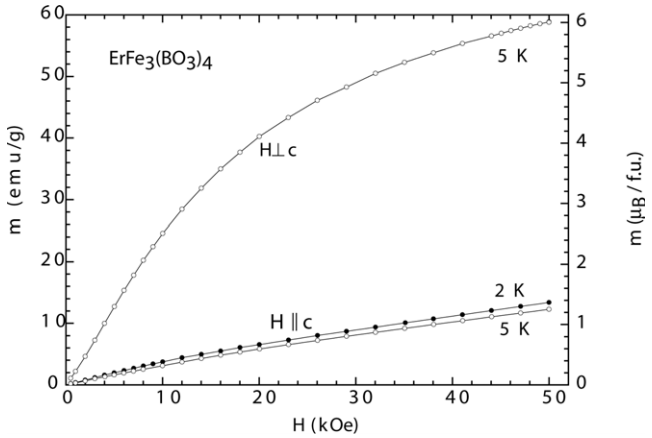

Figure 11. Magnetic field dependences of $ErFe_3(BO_3)_4$ magnetization measured along the c-axis and in the basal plane.

1.5 K, respectively, with the 120° structure being the minority phase. Discussing the possible origin of the 120° phase, it is supposed that some local defects of the crystal structure—impurities, vacancies etc—could be a probable reason for a local magnetic anisotropy of the Er-sublattice being different from the anisotropy of the main phase. The contribution of this local anisotropy depends on the value of the Er-moment and is negligible above 10 K. Below 10 K, the value of the Er-moment increases strongly, leading to a simultaneous increase of the sample volume seeing the 120° phase. The magnetic moment value of Er at 1.5 K amounts in this model to $\mu_{Er} = 5.3(1)\ \mu_B$. Compared to the free ion value of Er^{3+} of 9 μ_B this value is considerably reduced, a situation already found for the rare earth moments in the corresponding Tb- and Ho-compounds [12, 13]. Contrary, however, to $TbFe_3(BO_3)_4$ and $HoFe_3(BO_3)_4$ where at 1.5 K the rare earth magnetic moment value has reached saturation, figure 9 clearly shows that in $ErFe_3(BO_3)_4$ the increase of the magnetic moment value of Er is far from having reached saturation at 1.5 K.

The information extracted from the neutron diffraction data on the magnetic structure of $ErFe_3(BO_3)_4$ was compared with the magnetic measurements on the single crystal. The temperature dependences of the magnetic susceptibilities measured for the directions of the external magnetic field $H \parallel c$ and $H \perp c$ are depicted in figure 10. No anomalies are found either at the Néel temperature or at $T = 10$ K for either orientation. A strong magnetic anisotropy is established: the magnetization measured in the basal plane, $m_\perp$, exceeds the one measured along the c-axis, $m_\parallel$, over the whole temperature region. The ratio $m_\perp/m_\parallel$ increases with decreasing temperature and approaches $m_\perp/m_\parallel \sim 6$ at $T = 5$ K. Taking into account that the magnetization measured is defined as a sum of the contributions of the Fe- and the Er-subsystems and that the Fe-contribution may be considered in a first approximation as isotropic, this difference can be explained by the anisotropy of the g-factor of Er^{3+} ions. Indeed, this anisotropy was found for Er^{3+} in *huntite* structure by optical spectroscopy: $g_x = 8.68$, $g_y = 10.14$, $g_z = 1.33$ [8]. It should be noted that the broad maximum of the susceptibility at $T \approx 80$ K (inset of figure 10) is only observable for $H \parallel c$. It could be related probably to a temperature induced repopulation of the two low-lying Kramers doublets as found in $DyFe_3(BO_3)_4$ [22]. There is no difference between zero-field-cooling and field-cooling data for either magnetic field orientation.

The field dependence of the magnetization for the magnetic field lying in the basal plane and along the c-axis is shown in figure 11, the right axis of which is given in Bohr magneton per formula unit. The magnetizations measured for $H \parallel c$ and $H \perp c$ directions differ strongly due to the aforementioned anisotropy of the g-factor. For both directions the dependence is nonlinear. For neither orientation of the external magnetic field is there an indication of spin reorientation or spin-flop transitions. This is in accordance with the results of the neutron diffraction study which clearly indicated the easy-plane anisotropy of $ErFe_3(BO_3)_4$ over the whole temperature region.

4. Summary

Neutron diffraction and magnetization studies of the iron borates $RFe_3(BO_3)_4$ (R = Pr, Er) were carried out as a function of temperature. $PrFe_3(BO_3)_4$ crystallizes in $P3_121$ while $ErFe_3(BO_3)_4$ keeps the crystallographic spacegroup $R32$ over the whole measured temperature range 1.5 K $< T <$ 520 K. The interatomic Fe–Fe distance along the helicoidal chain increases only by about 0.3% while the size of the RO_6 prisms increases by 9% when going from R = Er to Pr. This confirms the essential role of these chains in determining the similar magnetic properties (transition temperatures, propagation vectors) of the whole series of $RFe_3(BO_3)_4$ compounds. Below $T_N = 40$ K the Er-compound becomes magnetically ordered with the propagation vector $\tau = [0\ 0\ 1/2]$. Both the Fe- and the Er-sublattice order simultaneously adopt a collinear easy-plane arrangement of the magnetic moments. Below 10 K the magnetic moment value of the Fe-sublattice stays about constant at $\mu_{Fe} = 4.2\ \mu_B$

while a steep rise in the magnetic moment value of the Er-sublattice appears. This increase of the Er-sublattice magnetization is accompanied by the appearance of a second type of moment arrangement of the Er-sublattice. Forming a 120° type structure within the trigonal a–b-plane, it is attributed to a minority phase embracing about 10% of the sample volume at 1.5 K and is linked to possible local defects of the crystallographic structure. The Pr-compound orders magnetically below $T_N = 32$ K with $\tau = [0\ 0\ 3/2]$. As in the case of the Er-compound, this leads to a doubling of the crystallographic unit cell in the c-direction. Both sublattices, the Fe- and the Pr-sublattice, order again simultaneously in an easy-axis magnetic structure already found in $TbFe_3(BO_3)_4$ [12] and in $HoFe_3(BO_3)_4$ [13] below 6 K. Contrary to the case of the Ho-compound and similar to $TbFe_3(BO_3)_4$ the easy-axis anisotropy of the rare earth sublattice is already at T_N strong enough in $PrFe_3(BO_3)_4$ to overcome the easy-plane anisotropy of the Fe-sublattice. The relative orientation of Fe- and Pr-moments ($\mu_{Fe} = 4.3\ \mu_B$, $\mu_{Pr} = 0.8\ \mu_B$ at 1.5 K) within the individual a–b-layers is parallel and therefore different from the situation in the Ho- and the Tb-compounds where the relative orientation is antiparallel. This can be explained using the results of Popova [21] and the spin–orbit coupling, leading to $J = |L - S|$ for light (Pr) and to $J = |L + S|$ for heavy lanthanides (Tb, Ho).

Acknowledgments

This work was supported by RFBR, grant no. 10-02-00765, and by the Physical Sciences Department of RAS, project no. 1.1.1.1.

References

[1] Balaev A D, Bezmaternykh L N, Gudim I A, Temerov V L, Ovchinnikov S G and Kharlamova S A 2003 *J. Magn. Magn. Mater.* **258/259** 532
[2] Zvezdin A K, Vorob'ev G P, Kadomtseva A M, Popov Y F, Pyatakov A P, Bezmaternykh L N, Kuvardin A V and Popova E A 2006 *JETP Lett.* **83** 509
[3] Kadomtseva A M, Popov Y F, Vorob'ev G P, Mukhin A A, Ivanov V Y, Kuz'menko A M and Bezmaternykh L N 2008 *JETP Lett.* **87** 39
[4] Zvezdin A K, Kadomtseva A M, Popov Y F, Vorob'ev G P, Pyatakov A P, Ivanov V Y, Kuz'menko A M, Mukhin A A, Bermaternykh L N and Gudim I A 2009 *JETP* **109** 68
[5] Chaudhury R P, Yen F, Lorenz B, Sun Y Y, Bezmaternykh L N, Temerov V L and Chu C W 2009 *Phys. Rev.* B **80** 104424
[6] Pankrats A I, Petrakovskiĭ G A, Bezmaternykh L N and Bayukov O A 2004 *JETP* **99** 766
[7] Chukalina E P, Kuritsin D Y, Popova M N, Bezmaternykh L N, Kharlamova S A and Temerov V L 2004 *Phys. Lett.* A **322** 239
[8] Popova M N, Chukalina E P, Stanislavchuk T N and Bezmaternykh L N 2006 *J. Magn. Magn. Mater.* **300** e440
[9] Popova E A, Volkov D V, Vasiliev A N, Demidov A A, Kolmakova N P, Gudim I A, Bezmaternykh L N, Tristan N, Skourski Y, Büchner B, Hess C and Klingeler R 2007 *Phys. Rev.* B **75** 224413
[10] Volkov D V, Demidov A A and Kolmakova N P 2008 *JETP* **106** 723
[11] Fischer P, Pomjakushin V, Sheptyakov D, Keller L, Janoschek M, Roessli B, Schefer J, Petrakovskiĭ G, Bezmaternykh L N, Temerov V and Velikanov D 2006 *J. Phys.: Condens. Matter* **18** 7975
[12] Ritter C, Balaev A, Vorotynov A, Petrakovskiĭ G, Velikanov D, Temerov V and Gudim I 2007 *J. Phys.: Condens. Matter* **19** 196227
[13] Ritter C, Vorotyniv A, Pankrats A, Petrakovskiĭ G, Temerov V, Gudim I and Szymczak R 2008 *J. Phys.: Condens. Matter* **20** 365209
[14] Mo H, Nelson C S, Bezmaternykh L N and Temerov V T 2008 *Phys. Rev.* B **78** 214407
[15] Hinatsu Y, Doi Y, Ito K, Wakeshima M and Alemi A 2003 *J. Solid State Chem.* **172** 438
[16] Klimin S A, Fausti D, Meetsma A, Bezmaternykh L N, van Loosdrecht P H M and Palstra T T M 2005 *Acta Crystallogr.* B **61** 481
[17] Campá J A, Cascales C, Gutiérrez-Puebla E, Monge M A, Rasines I and Ruíz-Valero C 1997 *Chem. Mater.* **9** 237
[18] Levitin R Z, Popova E A, Chtsherbov R M, Vasiliev A N, Popova M N, Chukalina E P, Klimin S A, van Loosdrecht P H M, Fausti D and Bezmaternykh L N 2004 *JETP Lett.* **79** 423
[19] Rodríguez-Carvajal J 1993 *Physica* B **192** 55 http://www.ill.eu/sites/fullprof/php/downloads.html
[20] Fausti D, Nugroho A A, van Loosdrecht P H M, Klimin S A and Popova M N 2006 *Phys. Rev.* B **74** 024403
[21] Popova M N, Chukalina E P, Stanislavchuk T N, Malkin B Z, Zakirov A R, Antic-Fidancev E, Popova E A, Bezmaternykh L N and Temerov V L 2007 *Phys. Rev.* B **75** 224435
[22] Popova E A, Tristan N, Vasiliev A N, Temerov V L, Bezmaternykh L N, Leps N, Büchner B and Klingeler R 2008 *Eur. Phys. J.* B **62** 123